Available on CMS information server

CMS NOTE 2001/011

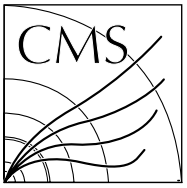

The Compact Muon Solenoid Experiment

CMS Note

Mailing address: CMS CERN, CH-1211 GENEVA 23, Switzerland

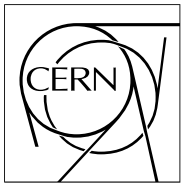

5 February 2001

Results on L2 trigger reconstruction in single and di-muon topologies

D. Acosta

Physics Department of the University of Florida, Gainesville, USA

G. Bruno

Physics Department of Pavia University, Pavia, Italy

T. Cox, J.R. Smith

Physics Department of University of California at Davis, CA, USA

M. Dallavalle, A. Fanfani, C. Grandi

Physics Department of Bologna University, Bologna, Italy

M. Fierro

Institute for High Energy Physics of the Austrian Academy of Sciences, Vienna, Austria

U. Gasparini, S. Lacaprara, P. Ronchese

Physics Department of Padua University, Padova, Italy

M. Konecki, N. Neumeister

CERN, Geneva, Switzerland

H. Rick

Physics Department of University of California, Riverside, USA

B. Tannenbaum,

University of California at Los Angeles, CA, USA

A. Vitelli

Physics Department of Torino University, Torino, Italy

R. Wilkinson

California Institute of Technology, CA, USA

Abstract

A detailed study of the CMS L2 trigger performance in single and di-muon topologies is reported, using the full detector simulation developed in CMSIM and the digitization, L1 trigger simulation and L2 reconstruction code developed in ORCA. The study was performed assuming the high luminosity scenario for the LHC machine ($L = 10\, nb^{-1}s^{-1}$). The resulting single muon and di-muon rates at L2 selection level are reported and compared with the L1 Global Muon Trigger output.

1 Introduction

The study of the performance obtainable by High Level Triggers (HLT) selection algorithms in CMS is of great importance in defining the design of the on line event filtering farm [1], which must accomplish the task of reducing the L1 Trigger rate (75 KHz) to the final output rate (100 Hz) suitable for data writing on mass storage. In particular, it is important to establish to which extent the background rate from minimum bias collisions passing the L1 trigger selection [2] can be reduced at a second trigger level (L2) using a fast processing of the digitized data from the muon and calorimeter systems alone (roughly the 25% of the whole event data), without using the Tracker information (supposed to be used only in a further on-line selection stage (L3)). Simple modelling of the CMS dataflow [3] shows that this multi-stage approach is convenient if L2 algorithms can assure a background reduction factor of the order of 10 w.r.t. the L1 output rate.

This note describes the detailed study of the performance of L2 reconstruction in the muon system, in conjuction with the full simulation of the L1 trigger system. A large amount of Monte Carlo generated data (about 10^6 events, divided in various background and signal datasets) was passed through the full CMS simulation (CMSIM) and reconstruction (ORCA) programs.

The note is organized as follows: Section 2 briefly describes the Monte Carlo data sets used, giving a few details on the simulation, digitization and reconstruction chain performed; Section 3 gives an overview of the muon L1 trigger processor, summarizing its main features and expected performance; Section 4 gives details on the digitization process simulated in the ORCA program, while Section 5 describes the L2 reconstruction in the muon system using the digitized data. Finally Section 6 reports the results on L2 trigger rates and selection efficiency in muon and di-muon final state topologies.

2 Monte Carlo data sets and detector simulation

Muonic triggers deal with muons (either *prompt* muons from heavy quarks and W/Z decays or *non-prompt* muons from pion/kaon decays) reaching the muon detectors at high rates (a few MHz), which must be rejected on the basis of a fast and precise momentum measurement, and by energy isolation cuts. Although punchthrough hadrons from pp collisions are predicted to give a hit rate comparable to that from real muons in the innermost stations of the muon detectors [2], they are expected to give an important contribution only to local track segments found in the early stages of the L1 trigger processors. They have thus been neglected in the present HLT study.

The input data generated for the muon L1 trigger and HLT studies was a sample of about 10^6 Monte Carlo fully simulated events, split into several data sets corresponding to the different physics processes summarized in Table 1.

The simulation and reconstruction chain was organized in several steps:

- the event generation step, based on the PYTHIA generator program [4], in which the kinematical properties of the event to be simulated and its stable particle content were determined;
- the simulation step, in which the full detector simulation using the CMSIM program [5], based on the GEANT 3 package [6], was performed and the particle hits in the sensing devices of the apparatus were obtained;
- the digitization step, in which the response of the apparatus to the particle hits was simulated, taking into account the piling-up of signals due to multiple interactions in the same or nearby bunch crossings with respect to the triggering event. This simulation part was implemented in the CMS object oriented reconstruction package ORCA (Object oriented Reconstruction program for CMS Analysis) [7]. This step gave digitized hits, input to the event reconstruction program;
- the L1 trigger simulation and HLT reconstruction starting from the digitized signals, performed by the ORCA program.

Details on the choise of the relevant parameters in the PYTHIA generator and GEANT3 in CMSIM, the GCALOR package [8] used for hadronic interactions, and the CMS detector geometry, can be found in [9].

As reported in Table 1, the bulk of the Monte Carlo production was devoted to the main source of background, given by *minimum bias* events having at least one muon in the final state with transverse momentum, p_T, high enough to reach the muon trigger system (3 GeV/c in the barrel region and 1.5 GeV/c in the endcaps). Although single muon triggers will necessarily have rather high p_T thresholds (in the 20-40 GeV/c range), it is important

Physics process	selection			nr. of events			cross-section	int. luminosity
	nr. of μ	$p_T^{\min}$	$\eta^{\max}$	generated	simulated	digitized	[mb]	[nb^{-1}]
MB, $\hat{p}_T = 0$	1	1.5	2.4	2524437	365139	160749	55.22	0.0448
MB, $\hat{p}_T = 5$	1	3.0	2.4	1234425	201435	114496	25.65	0.0457
MB, $\hat{p}_T = 10$	1	4.0	2.4	1170638	210082	135016	2.66	0.4405
MB, $\hat{p}_T = 20$	1	10	2.4	1146085	42637	35405	0.26	4.3012
MB, $\hat{p}_T = 10$	2	8,4	2.4	2439948	66018	61198	0.033	72.943
MB mix, $\hat{p}_T = 10$	2	8,4	2.4	1499400	48750	44237	0.26	5.797
W + jets	1	3	2.4	584686	49000	49000	$1.85 \cdot 10^{-4}$	3161.9
Z + jets	1	3	2.4	441589	27500	27500	$5.53 \cdot 10^{-5}$	7978.8
$Z^*\gamma$ + jets	1	3	2.4	899205	49000	49000	$1.00 \cdot 10^{-3}$	898.0
$WW/WZ/ZZ$	2	3	2.4	1759296	10000	10000	$6.79 \cdot 10^{-6}$	$6.8 \cdot 10^5$
$t\bar{t}$	2	3	2.4	102316	9500	9500	$6.22 \cdot 10^{-7}$	$1.6 \cdot 10^5$
$H \to WW \to 2\mu 2\nu$	2	3	2.4	25000	25000	25000	$3. - 11. \cdot 10^{-11}$	$1.6 \cdot 10^7$
$H \to ZZ \to 4\mu$	2	3	2.4	22000	22000	22000	$0.8 - 2.2 \cdot 10^{-12}$	$2.0 \cdot 10^{10}$

Table 1: Generated Monte Carlo datasets.

to generate and simulate the behaviour of potentially triggering muons of rather low p_T occurring at very high rates. This was intended to study the feed-through effect due to detector resolution and non-Gaussian tails in the reconstructed momentum distributions at L1 and L2 trigger stages, expected from *non-prompt* muons from $\pi^{\pm}/K^{\pm}$ decays and/or from multiple scattering in the detector. With this aim, four different samples of *minimum bias* events with a single muon in different p_T regions were generated, using different values of the minimum accepted p_T of the hard process at parton level, $\hat{p}_T$, as defined in the PYTHIA generator, to optimize the event generation. Further, each generated event was forced to have at least one muon, following a special weighting procedure described in [9].

An important source of background with more than one muon is random overlapping of two (or more) events with muons within the same bunch crossing. This contribution, which becomes more important at higher luminosity and lower transverse momentum thresholds, was taken into account in a dedicated dataset ("MB mix" in the Table).

Other sources of background, particularly important in the high p_T regions, are W/Z bosons and top quark production. No weighting procedure was applied in these samples and no direct semi-muonic decay of W/Z was forced at generation level. The final state muon(s) required to select events before the detector simulation stage could originate from direct heavy boson, top decays or from b, c quark decay chains.

Finally, signal samples of Standard Model Higgs production in the $ZZ^{(*)} \to 4\mu$ and $WW^{(*)} \to 2\mu 2\nu$ decay channels were also simulated, as bench-mark channels for efficiency studies, with five different values of the generated Higgs mass.

The realistic simulation of signals in the detector at LHC luminosities requires at digitization stage the piling-up of events occurring in the same or nearby bunch crossings with respect to the triggering events, as will be discussed in the following section. This task was accomplished by simulating a special sample of 10^5 minimum bias events with no muons in the final state, from which the set of events to be piled-up to a given triggering event was randomly chosen.

Total single-muon differential cross-sections and integral rates at the digitization level, together with the muon sample composition, are shown in Fig. 1. Rates are computed for the LHC luminosity $L = 10^{34}\text{cm}^{-2}\text{s}^{-1}$. As shown in Fig. 1, the *non-prompt* muon component is dominant in the low p_T region, decreasing from roughly 80% to 10% in the p_T range from 2 to 20 GeV/c.

The resulting total di-muon integral rates at the digitization level are shown in Fig. 2, as a function of the threshold on the transverse momentum of the lowest p_T muon, for the threshold on the highest p_T muons set at 8 GeV/c. Again, rates are computed for the LHC luminosity $L = 10^{34}\text{cm}^{-2}\text{s}^{-1}$.

3 Signal digitization

The digitization of the simulated hits (i.e. the creation of what corresponds to the 'raw data' in the real experimental environment), which requires the piling-up of the signals from the 'underlying' non-triggering events in the same or nearby machine bunch-crossing, was performed within the CMS OO reconstruction program ORCA (Object

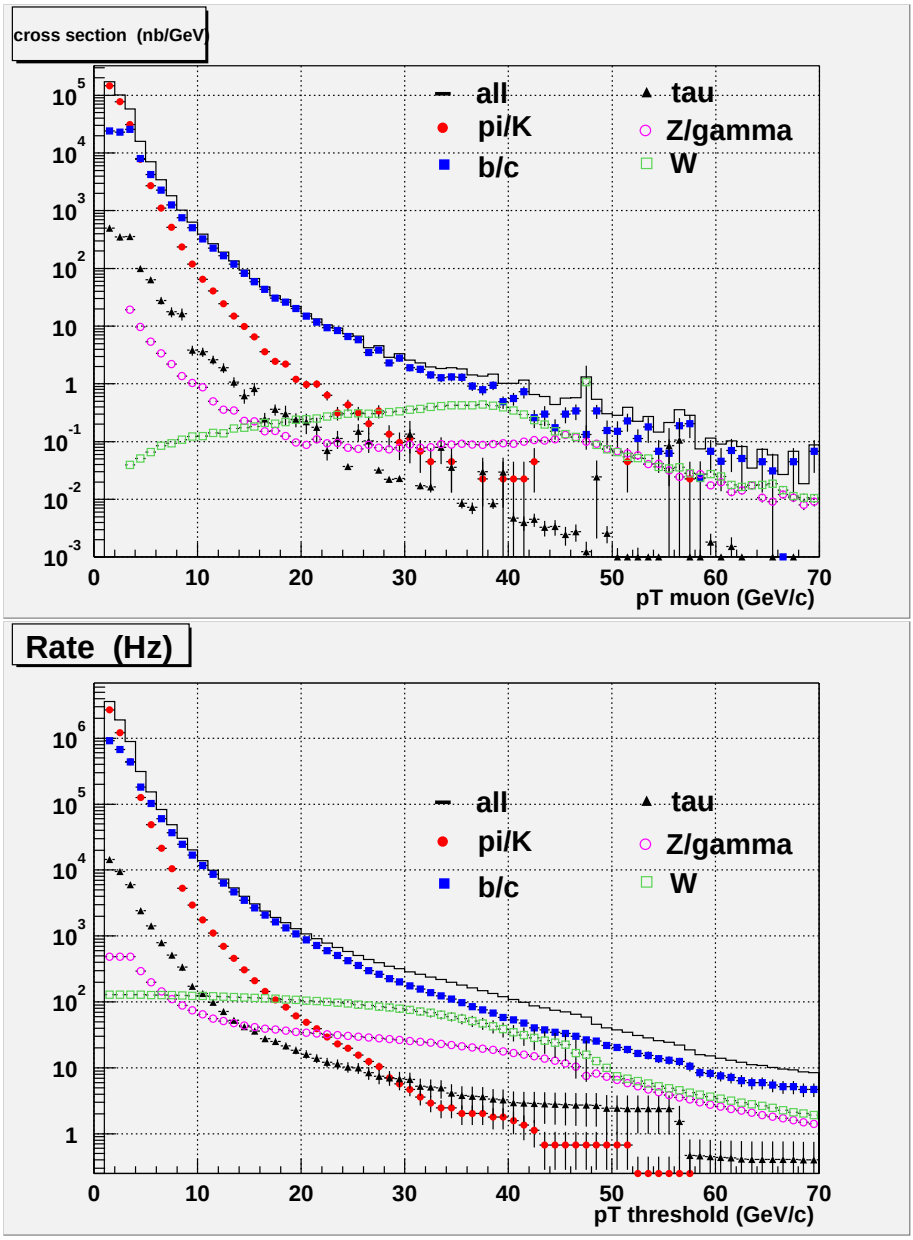

Figure 1: Differential cross-section and integral rates, at digitization level, for the different origins of the muon in the single muon sample.

oriented Reconstruction program for CMS Analysis) [7]. The underlying interactions, stored in an Objectivity database, were piled-up on the triggering event using Poisson statistics. To avoid trigger double counting these events were pre-filtered at generation level, skipping events having muons with $p_T > 3$ GeV/c which could themselves trigger the system.

At the LHC design luminosity of 10 nb^{-1}s^{-1} the total inelastic cross section of 55 mb, predicted by PYTHIA, implies an average number of 17.3 minimum bias events per bunch crossing, taking into account that about 20% of the bunches will be empty. The effect on the HLT selection of events with real muons occurring in off-time bunch crossings with respect to the triggering event, within a typical time-window for the electronic signal to be collected and shaped in the muon sub-detectors[1)] is estimated to be small, and was neglected in the present HLT studies. Only in-time bunch crossing event pile-up, relevant for the track matching studies to be performed at the third trigger level, was then simulated in the muon and tracker systems of CMS. On the other hand, the calorimetric

[1)] The maximum drift time in the barrel DT system is 360 ns, while a typical gate set in the CSC front-end electronics is 150 ns.

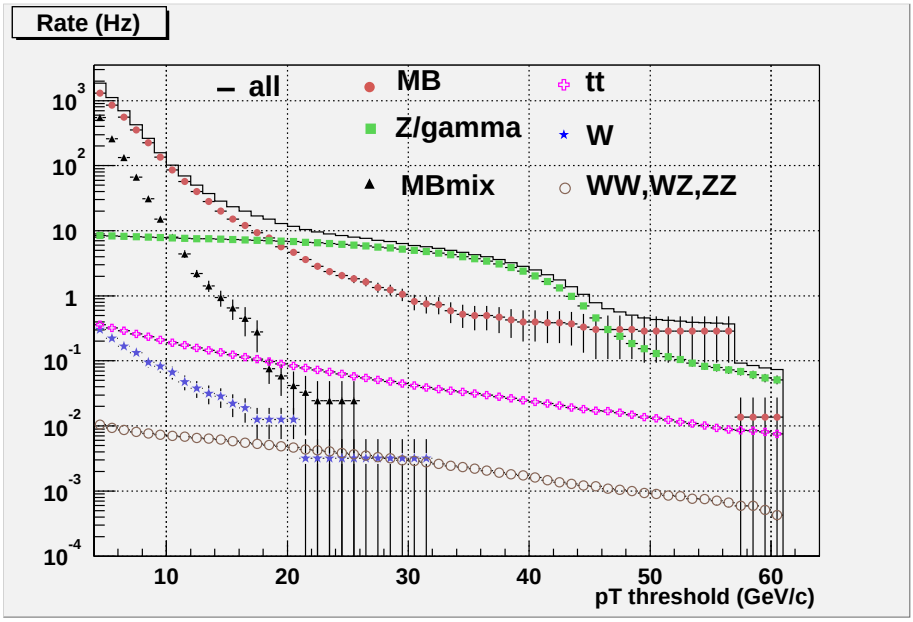

Figure 2: Integral rates for events with at least two muons delivering hits in the CMS muon detector, as a function of the threshold on the lowest p_T, for $p_T^{\rm high} > 8$ GeV/c. Dataset names are as in Table 1.

energy deposits around the triggering muon directions, relevant to study the effect of energy isolation cuts at the second level of the trigger, are affected by the occurrence of events in bunch crossings different from the triggering one. Following the dedicated studies on calorimetric triggers [10], a window of [-5,+3] bunch crossings was opened in the simulation of the calorimetric part of the digitization process.

In the barrel DT chambers, particular care was taken in simulating the behaviour of the drift cells as a function of the muon particle direction and impact position w.r.t. the sense wire, and of the residual magnetic field expected in the air gaps of the magnet iron yokes, where the chambers are situated. A schematic drawing of the cell with the drift lines in two different magnetic field configuration is shown in Fig. 3. The results of the study of the cell response based on dedicated simulation with the GARFIELD package [11] were parametrized in terms of an 'effective drift velocity' and included in the digitization simulation. The resulting drift time determined the TDC output signal used for the hit reconstruction. The accuracy of the parametrization w.r.t. the full simulation of the cell was within a few ns over the whole range of interest [12]. The full simulation was performed with the cell design described in the Muon TDR [13]; the results were linearly rescaled to the new cell size (4.2 cm instead of 4.0 cm) recently adopted for the final design of the barrel muon chambers.

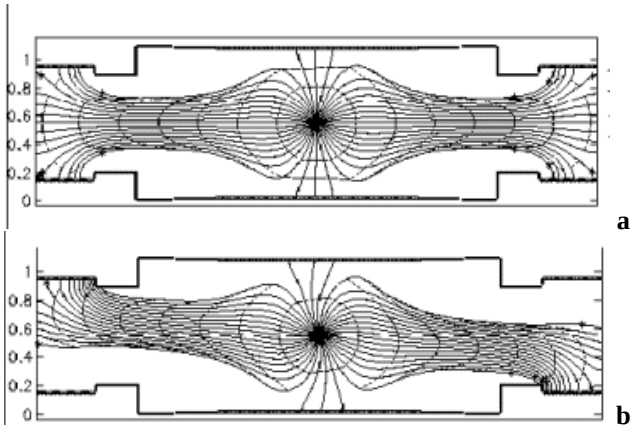

Figure 3: Drift lines in the muon barrel drift cell for different magnetic field configuration (from [12]): a) B=0.5 T perpendicular to the sense wire; b) B=0.5 T parallel to the sense wire.

In the endcap CSC's, the GEANT thin-layer approximation was used to model energy loss in the gas. This uses

the atomic structure of the gas molecules in the calculation of the collision cross section. Each ionizing collision along the path of the primary muon through the gas produces a free electron. Further delta electrons may be produced, and each electron is transported to the neighbouring anode wire according to the local electric and magnetic fields. Electron losses are taken into account due to the attachment coefficients in the $Ar/CO_2/CF_4$ gas mixture. Gas multiplication occurs in the vicinity of the anode, with fluctuations in the avalanche size. To create the analog signals seen by the wire and strip electronics, parametrizations of the amplifier and shaper response are used. These convolute in the ion drift collection time. Note that the signal may contain contributions from drifting electrons due to background hit from other beam crossings. Cross-talk between neighbouring strips has not yet been simulated, but this is generally small. Each strip which satisfies the L1 Trigger comparator logic causes the readout of a group of 16 strips. Within such a group, noise is simulated on empty strips which are neighbouring of a signal strip, and remaining empty strips are suppressed. A read-out dead time of 200 ns is assumed. Finally, the storage of the strip signals in Switched Capacitor Arrays (SCA) is simulated. The signal shape is sampled and stored at 8 times, each 50 ns apart. A noise contribution is added to each SCA sample. These samples are used for CSC hit reconstruction [13].

The RPC response was assumed to take place 20 ns after the passage of a charged particle through the detector with a Gaussian distributed jitter of 3 ns, which also accounts for the contribution from the front end electronics and the cables to the link board [14]. The 20 ns wide time gates were optimally adjusted in order to accomodate triggering signals. No cluster size effects have been considered in the current simulation, i.e. the passage of a charged particle through an RPC causes only one strip to give rise to a signal, and the intrinsic chamber noise was not simulated. It's worth to stress that the impact of these effects on the L1-GMT response and the subsequent HLT selection is yet to be studied.

4 L1 trigger simulation

The Level 1 muon trigger system of the CMS experiment will be implemented using specially designed hardware. It is a complex and redundant system, based on three independent detectors: the Drift Tube (DT) chambers in the barrel region ($|\eta| < 1.15$), the Cathod Strip Chambers (CSC) in the endcap region ($1.04 < |\eta| < 2.4$) and the Resistive Plate Chambers (RPC) in almost the whole acceptance region of the muon detector ($|\eta| < 2.1$).

The logical layout of the CMS L1 Trigger system is shown in Fig. 4. Its detailed description may be found in [2]. In the following the functional components of the Muon Trigger systems are briefly reviewed.

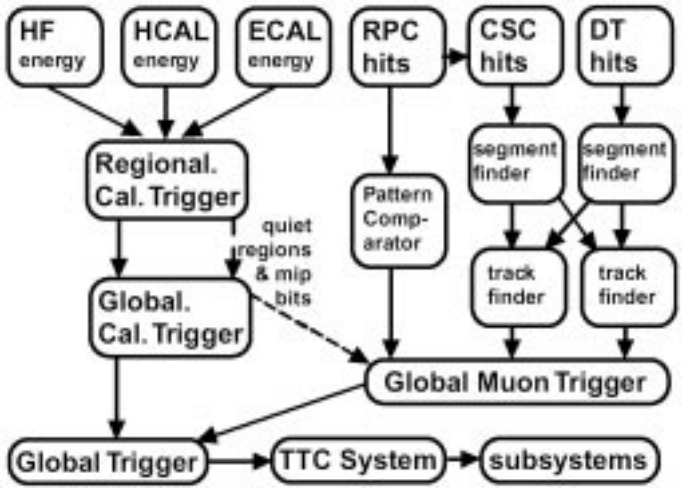

Figure 4: Block diagram of the L1 trigger system.

4.1 DT L1 trigger

The CMS Barrel Muon detector consists of four stations of DT chambers [13]. Each muon chamber is made up of 3 sets of drift tubes. Each set is composed of 4 layers of tubes (superlayer). Two superlayers measure the R-Φ coordinate and the third one the R-θ coordinate. The first step of the trigger system is the Bunch and Track Identifier (BTI). The BTI finds alignments of hits in each quadruplet and determines the LHC bunch crossing in

which the muon was produced, using a mean-timer technique. The second step is the TRAck COrrelator (TRACO) which associates two segments found by the BTI's sensible to the R-Φ coordinate. The last step performed by the on-chamber trigger is the Trigger Server (TS), which selects the two best TRACO segments in a chamber and passes them to the Regional Trigger. The segments found by the BTI's in the R-θ quadruplet are sent to the Trigger Server Theta (TST) which packs them in bit streams that are then used by the Regional Trigger to find alignments in the longitudinal view. The R-θ segments are also used by the TRACO to validate its R-Φ candidates. Details of the software OO implementation of the simulation can be found in [15].

The Regional Trigger is based on a Track Finder algorithm, which performs the task of building muon track candidates using the track segments of the local trigger (TRACO) output, assigning to them a momentum value by measuring the track curvature in the magnetic field. The task is achieved by a three-steps process (pair matching and extrapolation, track assembling, p_T assignment), as described in [2]. The 4 highest p_T muon candidates found are delivered to the Level-1 Global Muon Trigger (GMT).

4.2 CSC L1 trigger

The Encap Muon system of CMS [13] consists of four stations at each end of the CMS detector. Each station is composed of CSC of trapezoidal shape arranged to form a disk, with an azimutal coverage of 10^o or 20^o. In each chamber there are six layers of cathode strips aligned radially and anode wires aligned in the orthogonal direction.

Signals from the front end electronics boards are sent to a comparator network which locates the centroids of the strip charge clusters. These are fed to the cathode local CSC trigger processor (CLCT), while discriminated anode wire signals are sent to the anode local CSC trigger processor (ALCT). LCT cards search for valid track patterns, named LCT track primitives, in the six layers of a station. CLCT and ALCT primitives are associated in the Trigger Mother Board (TMB) and sent to the sector processor, covering a 60^o sector at each CSC endcap, where the CSC Track Finder algorithm is performed. The CSC Muon Sorter collects the track candidates from the sector processors and send the four best candidates to the Level-1 GMT. A detailed description of the system can be found in [16].

4.3 RPC L1 trigger

Both the Barrel and Endcap muon detectors are equipped, in addition to the DT and CSC systems, with RPC's as independent triggering devices [13]. Six layers of double gaps RPC's are mounted in the Barrel (2 layers for each of the 2 innermost DT stations, and one layer for each of the two outermost ones), while there are four layers in each Endcap. Details on the RPC geometry and the RPC trigger segmentation can be found in [17]. The RPC trigger is a Pattern Comparator Trigger (PACT) based on spatial and temporal coincidence of hits in four RPC muon stations, as described in [2]. The PACT delivers to the Global Muon Trigger 4 high-p_T muon candidates from the barrel and a total of 4 from the two endcaps combined.

4.4 Global Muon Trigger (GMT)

The GMT has two logical boards which process in parallel the DT and RPC barrel muons and CSC and RPC forward muons respectively, according to the muon merging and sorting logic described in detail in [2]. In the current simulation, the final GMT selection was set as described in [2], realizing a good compromise between the need for maximizing the triggering efficiency and acceptable trigger rates. In particular, muon candidates of any quality delivered from the DT and CSC TrackFinders were required to be confirmed by the RPC system for $|\eta| > 0.91$ and $|\eta| < 1.06$ respectively. This selection results in an overall L1 efficiency of 96% with a ghost fraction of the order of 0.2% [2].

5 L2 Trigger muon reconstruction

The local muon track reconstruction algorithm developed in the framework of the ORCA program for the Level 2 trigger [18] is seeded by the results of the L1 Global Muon Trigger. This is a "state vector" (position, direction and momentum) defined at the second station (either in barrel or endcap): it's extrapolated to a (virtual) surface inside the muon system, and "measurements" are first collected going outward the detector iron yoke using the GEANE package [19], taking into account the muon energy loss in the material and the effect of the multiple scattering. The L1-GMT estimation of the momentum was used in this stage for the track propagation in the magnetic field.

On the chamber compatible with the propagation a fast local pattern recognition using the reconstructed hits from digitized signals in DT and CSC detectors is initiated. In the barrel chambers a simple least square fits to straight lines is performed, separately for R-Φ and R-θ, delivering 2 dimensional segments: these are eventually associated to build a 3-D segment in space. The endcap chamber hits are 3 dimensional, so a 3-D linear fit is performed. Up to 12 (6) points per track segment are included in the barrel (endcap) chambers, corresponding to the maximum number of the chamber measurement layers. Hit sharing between segments is not allowed, and ambiguities are resolved on the basis of a maximum number of hits and best χ^2 criterion.

The predicted state vector at the next measurement surface was compared with existing measurement points and accordingly updated using a Kalman filtering technique, as described in [20]. During the outward propagation a loose cut on incremental χ^2 is applied. The algorithm aims to improve the state vector defined by L1 and have an unbiased momentum estimation (the one delivered by L1 is biased because of the 90% efficiency threshold definition there adopted).

In the barrel chambers, the reconstructed segments were used as 'measurements' at each stage of the Kalman filtering procedure, whereas in the endcap chambers single reconstructed points belonging to the predefined pattern determined by the track segments were used.

The procedure is iterated up to the outermost station, where the propagation is reversed, going now inward, but applying a tighter cut on incremental χ^2 to reject bad measurements, up to the innermost station, where the track parameters and their errors are delivered as the parameters of "muon track candidate" of the L2 reconstruction.

These will be used for extrapolation, matching and/or global fitting with the Tracker detector in the subsequent (Level 3) trigger stage. Moreover, to improve the momentum resolution, a constrained fit assuming that the muon candidate originates from the interaction region is performed using the muon detector alone; the beam spot size($\sigma_{xy} = 15$ μm, $\sigma_z = 5.3$ cm) was assumed as the uncertainty on the primary vertex position. The resulting determination of the transverse momentum was used in the L2 selection algorithm to reject or accept the event for the further L3 processing.

The efficiency of the L2 reconstruction as a function of the generated muon transverse momentum is shown in Fig. 5,a for muons in the pseudorapidity range $|\eta| < 2.4$. The efficiency vs η for muons with $p_T > 7$ GeV/c is shown in Fig. 5,b. It must be stressed that in the present version of the code no attempt has been made to use the RPC detector signals in the L2 algorithm. This causes large inefficiency in the most difficult region between the endcap and the barrel systems, as can be seen by comparing the L2 efficiency with the GMT L1 efficiency also reported in the figure.

Fig. 6,a shows the distribution of the quantity $(p_T^{rec} - p_T^{gen})/p_T^{gen}$, where p_T^{gen} and p_T^{rec} are the generated and reconstructed transverse momentum respectively. The reconstructed momentum is the result of the constrained vertex fit discussed above. The improvement in the resolution w.r.t. the L1 result is evident [2)]. However, in the barrel-endcap overlap region and in the region at $|\eta| > 2$ the momentum resolution is worse, as shown by the scatter plot in Fig. 6,b. As it can be seen in Fig. 7, the L2 p_T resolution is about 10% in the barrel region and slightly worse, 14%, in the endcap region for $1.3 < |\eta| < 2.1$. In the 'overlap' ($0.9 < |\eta| < 1.3$) and in the very forward ($|\eta| > 2.1$) regions, the resolution is 17% and 21% respectively.

6 L2 Trigger selection and results

The integral trigger rate for single muons obtained in the minimum bias background sample is shown in Fig. 8 as a function of the threshold on the p_T reconstructed at L2; the corresponding L1 rate is also shown for comparison. The L2 rate was computed by imposing that both the L1 and L2 p_T estimates exceed the considered threshold. It can be seen that the improvement in the momentum resolution considerably reduces the feed-through into the high p_T region of the low p_T muons, thus reducing the trigger rate by almost one order of magnitude. In a few percent of the cases (mainly events in the tails of distribution of Fig. 6) the result of the vertex constrained fit was in large disagreement w.r.t. the estimate computed at the last measurement surface in the muon system, leading to unreliable momentum determination at L2. When the difference between the two p_T estimates divided by the p_T value of the L1 output was larger than 1.5, the L1 determination was instead used to evaluate the L2 trigger rate. As mentioned above, further code development (possibly including the RPC trigger information in the L2 algorithm) is needed in this case.

A reduction of the background from minimum bias events can be obtained exploiting an energy isolation cut on

[2)] The offset in the average value of L1 distribution is due to the 90% efficiency threshold definition adopted in the L1 trigger

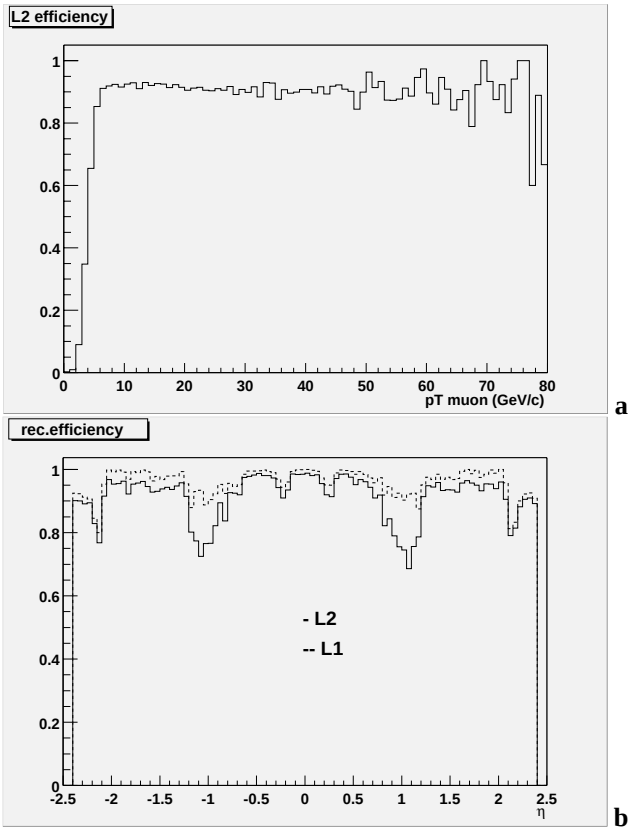

Figure 5: Level 2 trigger muon reconstruction efficiency. In the lower plot, the L1-GMT efficiency is also shown (dashed line).

the reconstructed muon. Muons from pion and kaon or b/c decays are typically produced in jets which deliver electromagnetic and hadronic energy in the calorimeters, while muons from W/Z bosons or heavier objects are isolated. Unfortunately the difference in the calorimetric energy deposited in a cone around the muon between the two cases is reduced by the piling-up of energy from the underlying events, which is huge at high luminosity. The radius $R = \sqrt{\Delta\eta^2 + \Delta\phi^2}$ of the cone cannot be too large in order to minimize this pile-up effect. It was found that the value R=0.4 is the best compromise between the needs of minimizing the pile-up energy and maximizing the collection of energy from the triggering event in which the muon is produced. This can be seen from Fig. 9, where the background rejection factor in different minimum bias samples obtained by cutting on the calorimetric energy in a cone of radius R is plotted against the selection efficiency obtained from the same cut applied to W decay events. The four cases correspond to minimum bias events containing a muon reconstructed at L2 with p_T bigger than 5, 10, 15 and 20 GeV/c respectively. Due to the pile-up effect, the difference in the collected energy between the background sample and signal samples from decays of heavy particles is small for minimum bias events with low momentum muons (where the pile-up energy from underlying events dominates). The difference is sizeable only for minimum bias events with relatively energetic jets containing high p_T muons (above 10 GeV/c). This is shown in Fig. 10, where the sum of electromagnetic and hadronic transverse energies collected in calorimetric towers in the cone with $R < 0.4$ around the triggering muon is shown for the single W/Z sample, the full minimum bias sample and the minimum bias sample with energetic muons ($p_T > 20$ GeV/c). It was then required that the sum of electromagnetic and hadronic transverse energies in the cone with $R < 0.4$ be less than 20 GeV. As shown from the plot with triangles in Fig. 8, a rate reduction factor of about 2 is achieved for muon p_T thresholds in the range 15-30 GeV .

The integral rates for di-muon triggers obtained at L2 as a function of the threshold on the highest p_T muon are shown in Fig. 11, for two different representative values of the lowest p_T threshold. The calorimetric isolation cut is not implemented in this case. It can be seen that for the di-muon final state topology the muon feed-through effect due to finite momentum resolution is less important than for the single muon topology. A background reduction factor of about 5 can anyway be achieved w.r.t. L1 rate. In the high luminosity scenario considered here, a L2 rate as low as 300 Hz is obtained for a moderately high asymmetric cut on the thresholds e.g $p_T^{(1)} > 15$ GeV/c, $p_T^{(2)} > 4$ GeV/c, as it can be seen from the Fig. 11,b. It's worth noting that the above di-muon rate is slightly underestimated

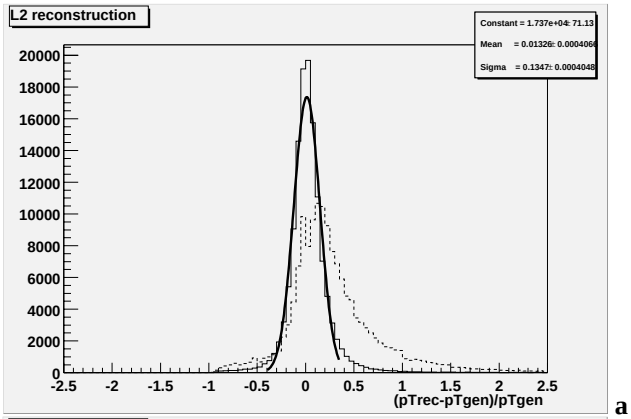

a

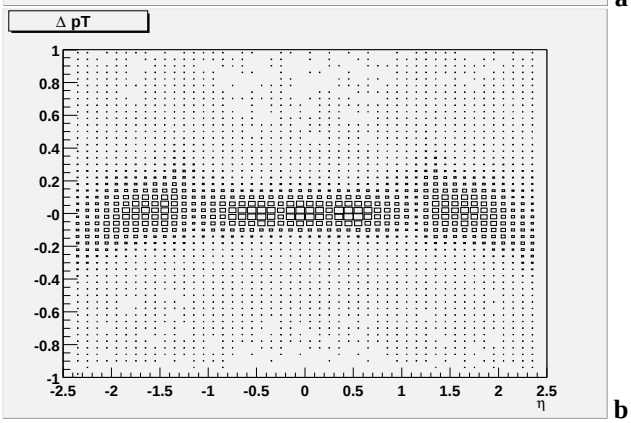

b

Figure 6: Resolution in the transverse momentum reconstruction in the Level 2 muon trigger. In the upper plot, the L1-GMT resolution is shown by the dashed line.

due to the fact that the Monte Carlo minimum bias di-muon data set considered in the present study (see Table 1) does not include muons below 4 GeV/c. The contribution from the feed-through of these low energy muons into higher p_T regions is then neglected in the rate plots.

The reconstructed di-muon invariant mass spectrum in the Z sample and the $H \rightarrow 4\mu$ invariant mass ($m_H = 180$ GeV) are shown in Fig. 12. The L2 invariant mass resolution on the Z boson is about 13%, consistent with the single muon resolution previously shown.

The di-muon differential rate as a function of the L2 reconstructed invariant mass is shown in Fig. 13. As seen in the figure, the asymmetric cut $p_T^{(1)}, p_T^{(2)} >$ (30,20) GeV/c leads to an integral rate of a few Hz, retaining the bulk of Z, double-bosons and $t\bar{t}$ production signals. For comparison, the $H \rightarrow WW \rightarrow 2\mu 2\nu$ signal has a rate about two orders of magnitude below that for the $t\bar{t}$ (for $m_H = 160$ GeV), with a similar invariant mass spectrum.

7 Summary and conclusions

The HLT capabilities of the CMS detector at the second level have been extensively studied using the detailed trigger simulation and reconstruction code developed in the CMS reconstruction program ORCA. The study was done assuming the high luminosity scenario. It has been shown that a background reduction of about one order of magnitude can be achieved w.r.t. the L1 output in single muon topologies by using the digitized data from the muon and calorimeter sub-systems. For a typical muon p_T cut set at 20 GeV/c in both the L1 and L2 trigger levels and requiring isolation of the muon w.r.t. the energy deposits in the calorimeters, a single muon rate of about 1 kHz is obtained.

For the di-muon topology, an L2 trigger rate as low as 300 Hz can be obtained requiring a moderately high p_T cut like $p_T^{(1)}, p_T^{(2)} >$ (15,4) GeV/c. Alternatively, only a doubling of the single muon L2 bandwidth is obtained by requiring a rather low momentum cut like $p_T^{(1)}, p_T^{(2)} >$ (8,4) GeV/c.

A fairly good resolution (about 13%) on the reconstructed invariant mass of heavy objects is obtained before processing the data from the tracker system, already allowing Z boson identification with good efficiency at L2.

Possible improvements of the L2 algorithm are under study; in particular, the possibility of integrating the RPC L1 trigger information in the L2 reconstruction is under development. In any case, the current code is a good starting point for the development and study of the 3rd level trigger algorithm with the inclusion of the processing of the tracker detector data. For the single muon trigger, this has to fulfill the task of further reducing the trigger output rate by more than one order of magnitude.

8 Acknowledgements

The authors wish to gratefully thank Vincenzo Innocente and David Stickland for the help in developing the simulation and reconstruction code in the new Object-Oriented CMS software environment and in the organization of the huge Monte Carlo simulation production required by the present study. The authors are also gratefull to Paris Sphicas and Grzegorz Wrochna for usefull discussions and suggestions.

References

[1] The CMS-DAQ System Technical Design Report, CERN-LHCC report, in preparation.

[2] The CMS-Trigger Technical Design Report, CERN-LHCC 2000/38, and reference quoted therein.

[3] CMS Workshop on High Level Triggers,
http://cmsdoc.cern.ch/cms/TRIDAS/distribution/Meetings/TriDAS.workshops/2000.07.21/Paris.Sphicas.1.pdf

[4] T. Sjostrand, *Pythia Ref. Manual*, CERN-TH 7112/93.

[5] http://cmsdoc.cern.ch/cmsim/manual/cms118/manual.html

[6] GEANT – Detector Description and Simulation Tool, CERN, Geneva, 1993.

[7] http://cmsdoc.cern.ch/orca/

[8] C. Zeitnitz, T.A. Gabriel, 'The GEANT-CALOR interface and benchmark calculations of ZEUS test calorimeters', Nucl. Instr. Meth. **A349**(1994) 106–111.

[9] N.Neumeister et al.,'Monte Carlo simulation for High Level Trigger studies in single and di-muon topologies', CMS IN 2000/053.

[10] C. Seez, 'Minimum-Bias Pileup Issues in Electron-Photon HLT Studies', CMS IN-2000/001.

[11] R. Veenhof, 'Garfield, a Drift-Chamber Simulation Program user's guide', CERN Program Library W5050, 1994.

[12] A.Gresele, T.Rovelli, 'Parametrization of B field effects in DT chambers', CMS note 1999/064.

[13] The Muon project Technical Design Report, CERN-LHCC 1997/32.

[14] G.Bruno, 'A simulation of the RPC muon trigger for CMS', CMS IN 1998/004.

[15] C.Grandi, 'Object Oriented simulation of the L1 trigger system of a CMS muon chambers', proceedings of CHEP 2000, p. 220

[16] S.M.Wang, D.Acosta, 'Simulation studies of the Transverse Momentum Resolution of the CSC Track-Finder', CMS IN 2000/026.

[17] G.Bruno et al.,'RPC System Geometry Simulated in CMSIM 118-120 and ORCA 4.2', CMS IN 2000/054.

[18] A.Vitelli, 'Object Oriented reconstruction in the CMS muon chambers', proceedings of International Conference on Computing in High Energy Physics, Padua, February 2000, p. 29.

[19] V.Innocente, M.Mairie, E.Nagy, GEANE, CERN/L3 report n. 572.

[20] U.Gasparini, L.Stanco, 'Track Finding and Global Reconstruction in the CMS Barrel Muon System', CMS TN/94-298.

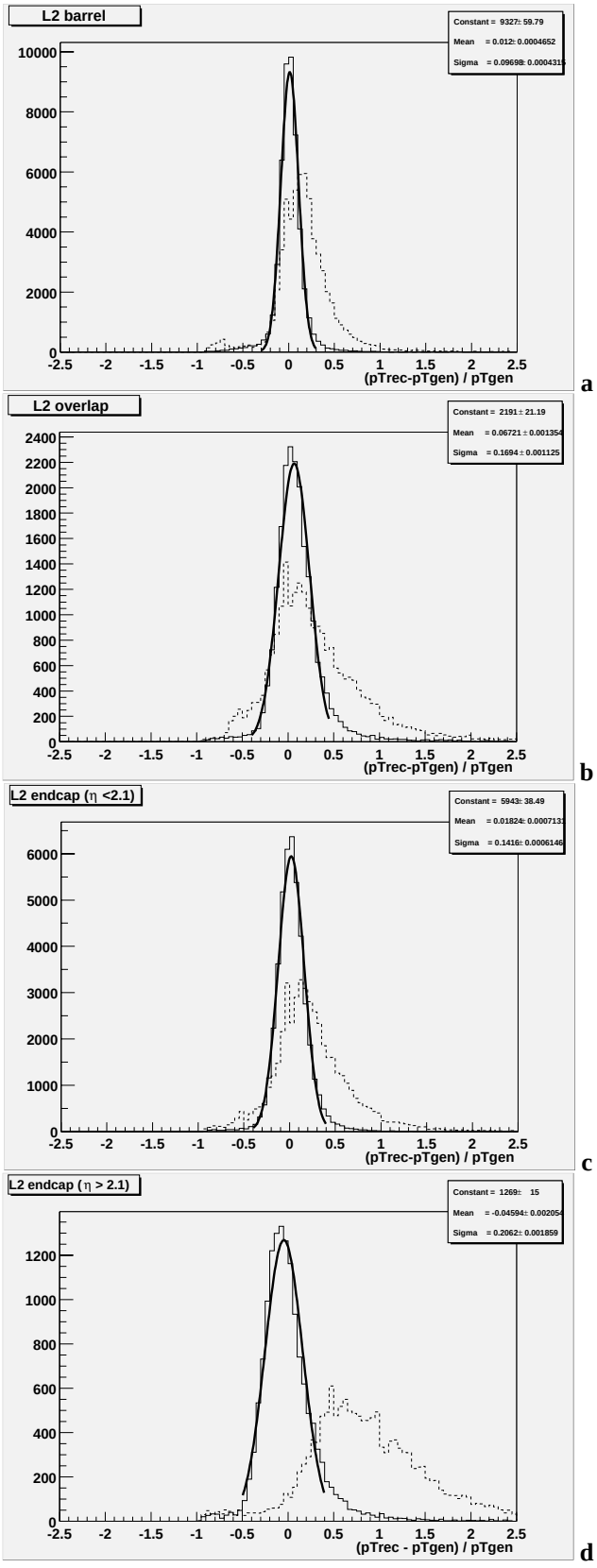

Figure 7: Resolution in the transverse momentum reconstruction in the Level 2 muon trigger for different η regions: a) barrel region ($|\eta| < 0.9$); b) 'overlap' ($0.9 < |\eta| < 1.3$); c) endcap ($1.3 < |\eta| < 2.1$); d) endcap ($0.9 < |\eta| > 2.1$). The L1-GMT resolution is shown by the dashed lines. All the plots are normalized to the same integrated luminosity.

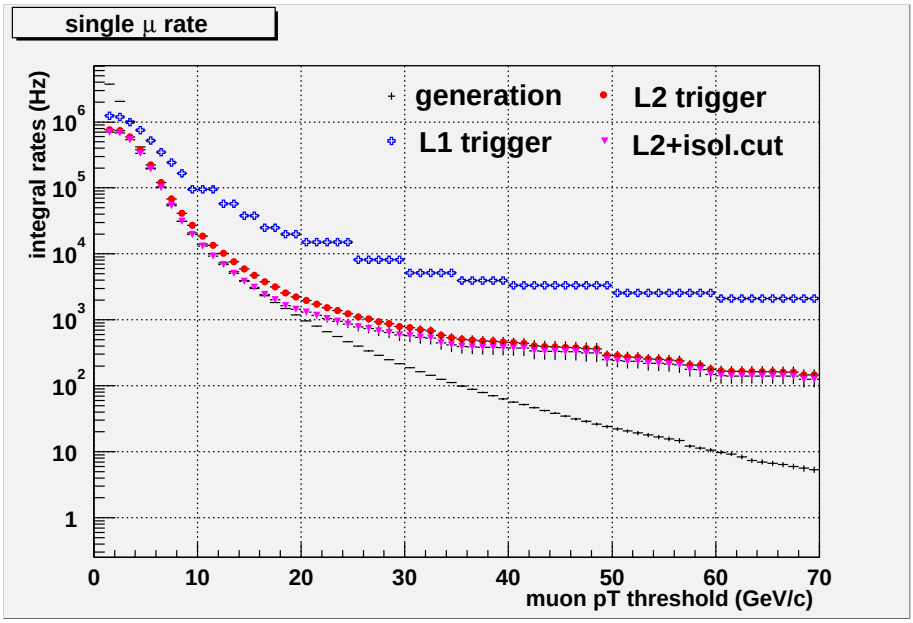

Figure 8: Single muon integral rates in the minimum bias background sample.

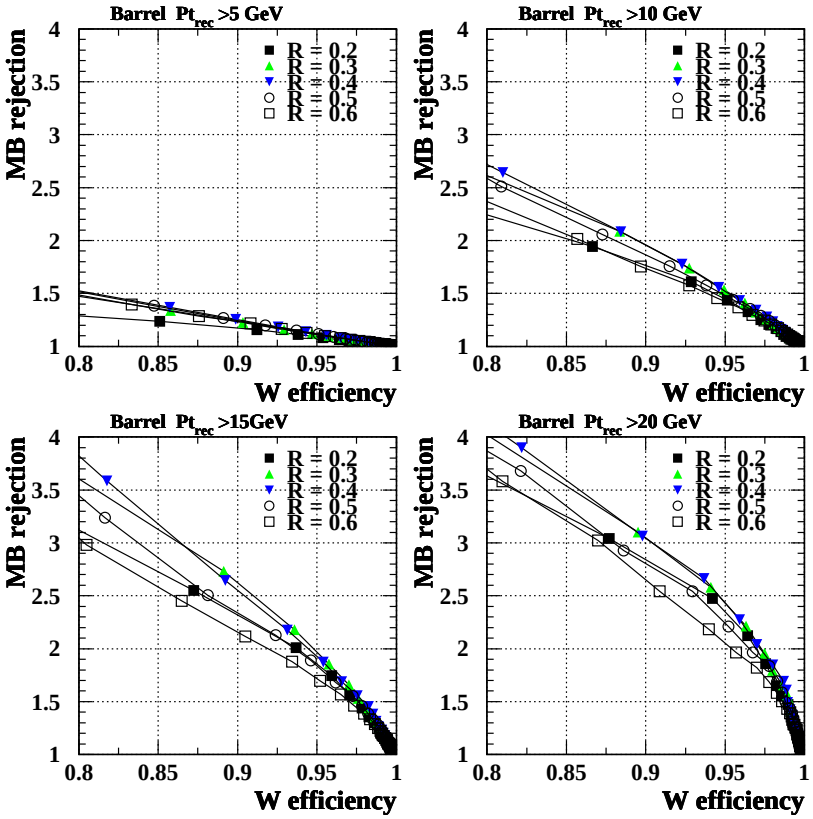

Figure 9: Background rejection factor vs W selection efficiency obtained by the energy isolation cut on the muon. The rejection factor refers to minimum bias samples containing a muon with reconstructed p_T above the four different thresholds: a) 5 GeV/c ; b) 10 GeV/c; c) 15 GeV/c; d) 20 GeV/c.

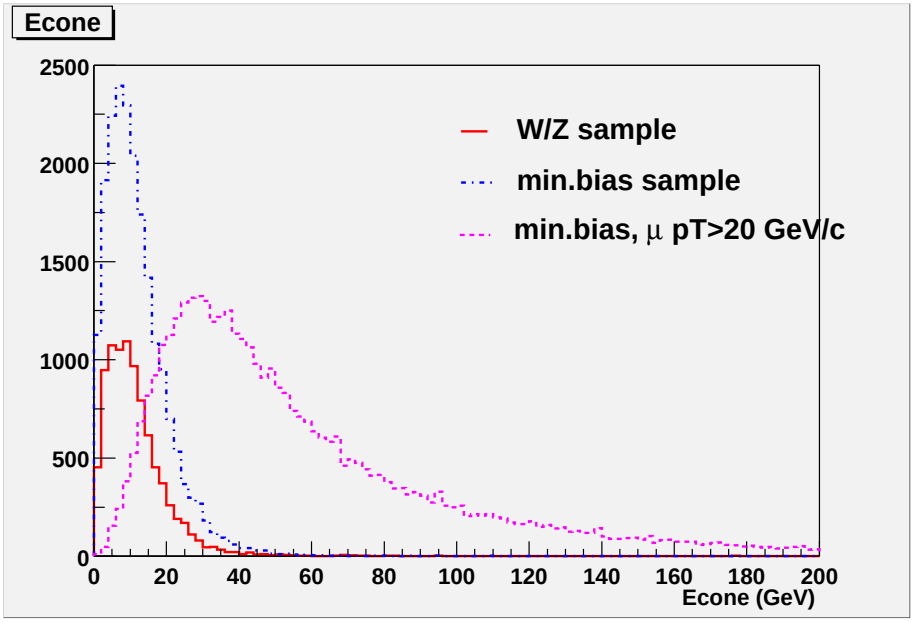

Figure 10: Calorimetric transverse energy in a cone with $R < 0.4$ around the triggering muon. Relative normalization between the samples is arbitrary.

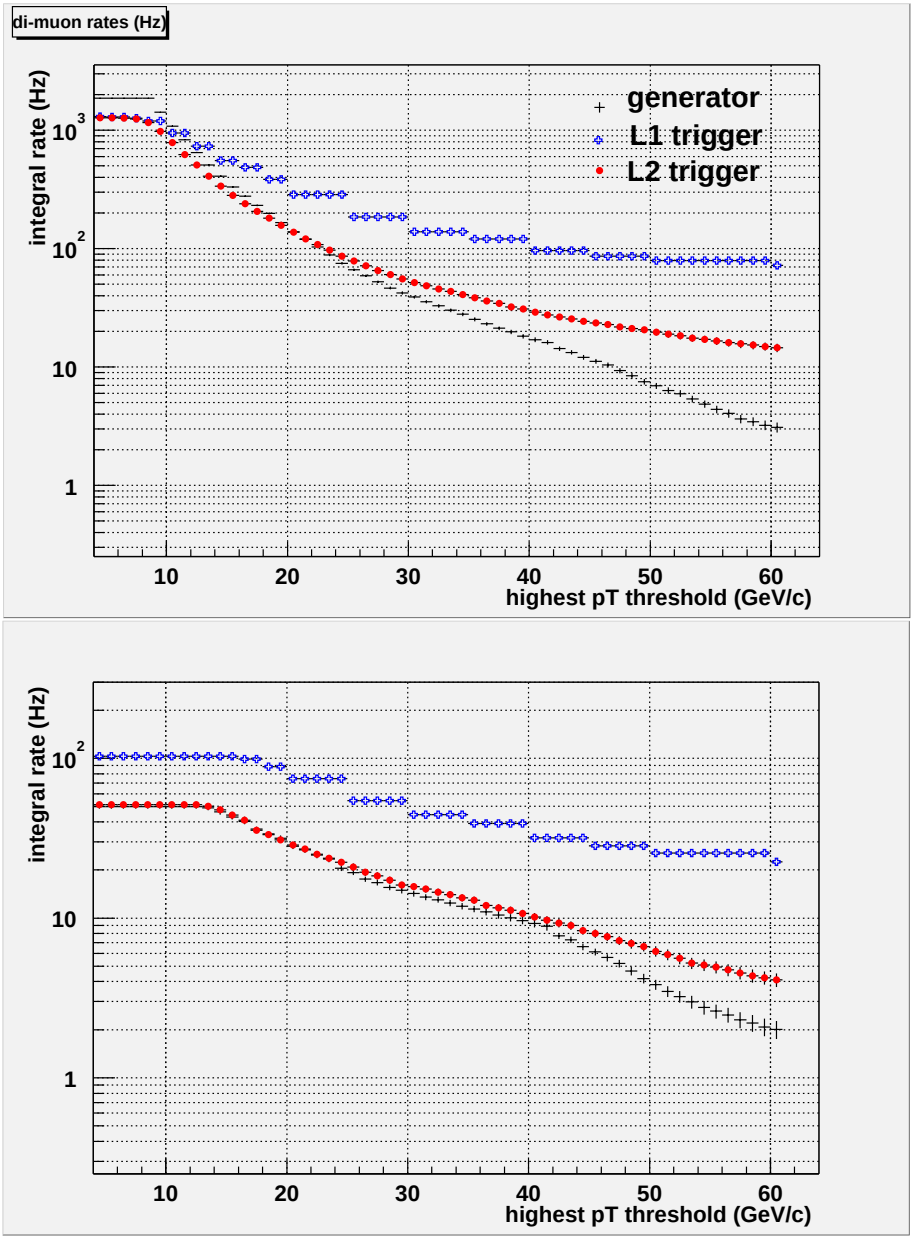

Figure 11: Di-muon integral rates for different threshold values of the lowest p_T muon: a) $p_T^{(2)} = 4\ GeV/c$; b) $p_T^{(2)} = 12\ GeV/c$.

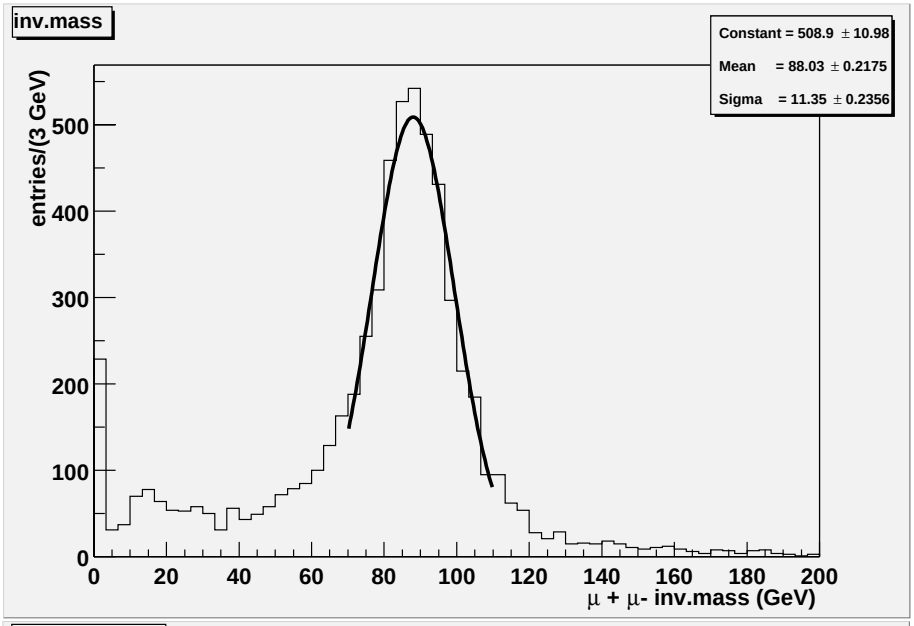

a

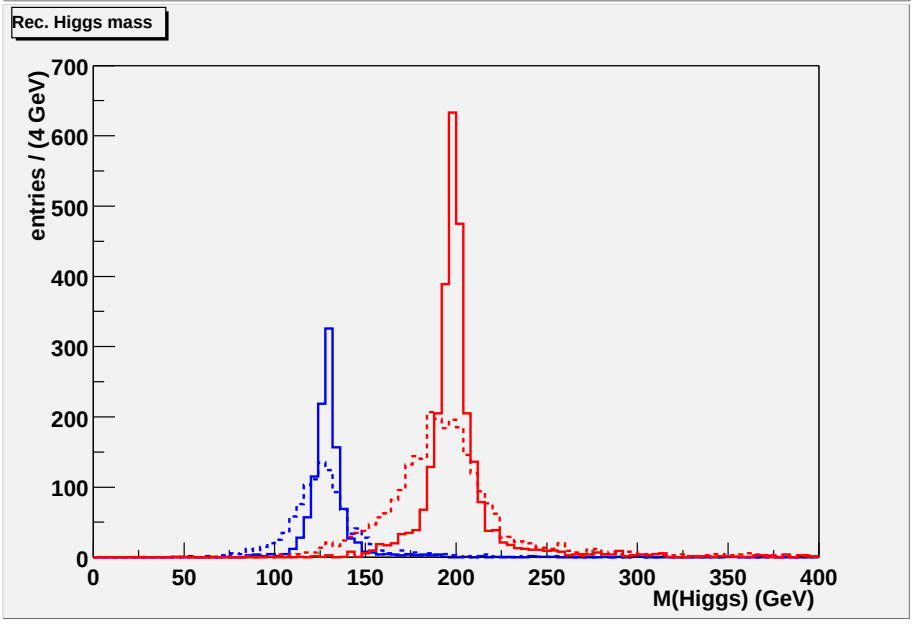

b

Figure 12: Invariant mass spectra as reconstructed at L2: a) di-muon invariant mass in single Z sample; b) Higgs invariant mass for M_H=130 (left plots) and 200 GeV (right plots) respectively. The dashed line plots show the results obtained using the reconstructed Z mass; the full line plots show the results obtained with the nominal Z mass value for the on-shell Z particles.

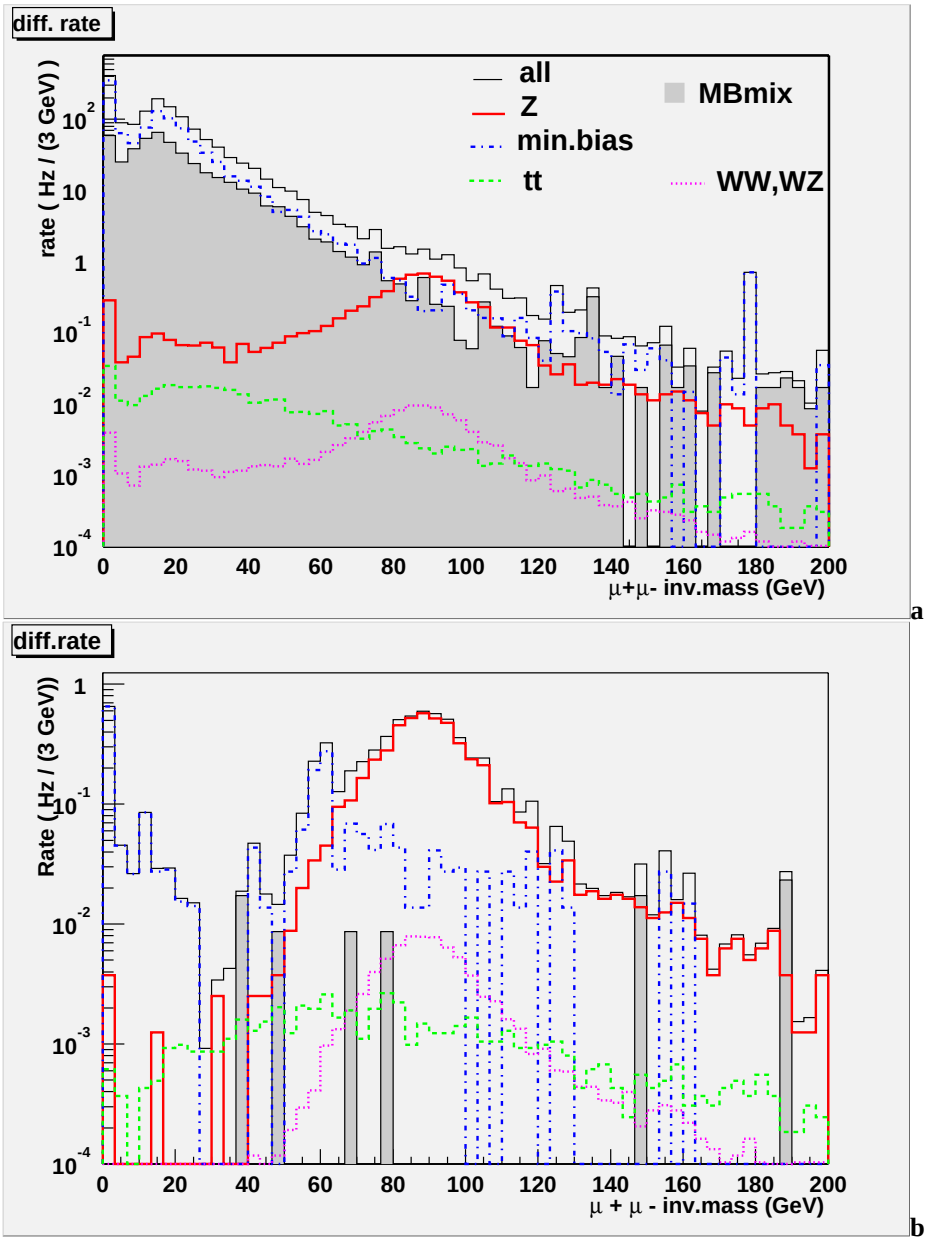

Figure 13: Differential rate vs reconstructed di-muon invariant at L2: a) with no p_T cut; b) with the asymmetric p_T cut: $p_T^{(1)} > 30\ GeV/c$, $p_T^{(2)} > 20\ GeV/c$.